Journal of Physics and Chemistry of Solids 73 (2012) 363–367

Contents lists available at SciVerse ScienceDirect

Journal of Physics and Chemistry of Solids

journal homepage: www.elsevier.com/locate/jpcs

Electrochemical supercapacitor studies of hierarchical structured Co^{2+}-substituted SnO_2 nanoparticles by a hydrothermal method

K. Karthikeyan [a], S. Amaresh [a], D. Kalpana [b], R. Kalai Selvan [c], Y.S. Lee [a,*]

[a] Faculty of Applied Chemical Engineering, Chonnam National University, Gwangju 500-757, Korea
[b] Central Electrochemical Research Institute, Karaikudi 630 006, India
[c] Solid State Ionics and Energy Devices Laboratory, Department of Physics, Bharathiar University, Coimbatore 641 046, India

ARTICLE INFO

Article history:
Received 25 February 2010
Received in revised form
25 September 2011
Accepted 29 September 2011
Available online 25 October 2011

ABSTRACT

Hierarchical structured Co-doped SnO_2 nanoparticles are prepared by a low temperature hydrothermal process. The structural and surface morphologies of the SnO_2 and $Sn_{1-x}Co_xO_2$ nanoparticles are studied by X-ray diffraction (XRD), Fourier transform infrared spectroscopy (FT-IR), transmission electron microscopy (TEM), and scanning electron microscopy (SEM). The $Sn_{1-x}Co_xO_2$ nanoparticles form with a tetragonal rutile structure during the hydrothermal process without further calcination. The pseudocapacitance behavior of the $Sn_{1-x}Co_xO_2$ nanoparticles is characterized by cyclic voltammetry (CV) in 1.0 M H_2SO_4 electrolyte. The specific capacitance (SC) is found to increase with an increase in cobalt content. A maximum SC of 840 F g^{-1} is obtained for a $Sn_{0.96}Co_{0.04}O_2$ composite at a 10 mV s^{-1} scan rate.

1. Introduction

It has been widely accepted in recent years that electrochemical supercapacitors (ECs) are the best candidates to provide high power density and excellent reversibility with a long cycle-life for new energy applications such as burst power generation, memory back-up devices, and hybrid vehicles [1]. Therefore, the development of suitable electrode materials for ECs to meet the requirement of high power and long durability is attracting much attention. Based on the charge storage mechanism, ECs can be divided into two types: (i) electrical double-layer capacitors (EDLCs) that utilize the capacitance arising from charge separation at an electrode/electrolyte interface, and (ii) pseudocapacitors that utilize the charge-transfer arising from redox reactions occurring on the surface of the electrode.

Pseudocapacitors are being widely investigated because of their large specific capacitance and high-energy properties. Since pseudocapacitance arises from the redox reaction of electroactive materials, transition metal oxides [2,4], and conductive polymers [5,6] with several oxidation states are considered promising electrode materials for pseudocapacitors. Among the metal oxides, anhydrous ruthenium oxide possesses high capacitance and excellent electrochemical reversibility [3]. Although RuO_2 gives high specific capacitance (SC), it has the disadvantages of high cost and toxicity. Therefore, an alternative electrode should be inexpensive and exhibit capacitive behavior similar to that of ruthenium oxide. Nanosized SnO_2 particles as an *n*-type semiconductor with a wide band gap (E_g=3.6 eV, at 25 °C) have been attracting much attention given their lower cost and environmentally benign nature. Nanosized SnO_2 has been used as promising gas sensors [7], electrodes for lithium ion batteries [8], and in dye-sensing solar cells [9].

It is well-known that one of the most common ways to modify the characteristics of a material is by introducing dopants into the structure. Doping with metal additives (Al, Co, Fe, and Cu) can lead to an increase in surface area of SnO_2-based powders [10,11], stabilize the SnO_2 surface, and promote a decreased grain size. In general, the Co dopant can inhibit growth of crystallite and plays an important role in the electrochemical properties. The Sb-doped SnO_2 nanocrystallites were prepared by a sol–gel method and an SC of 16 F g^{-1} obtained from a CV scan rate of 4 mV s^{-1} in 1.0 M KOH electrolyte [12]. The same authors have also studied the composite electrodes of SnO_2 and RuO_2, and an SC value of 33 F g^{-1} was reported at a CV scan rate of 50 mV s^{-1}. To the best of our knowledge, there are no reports in the literature regarding the usage of Co-doped SnO_2 as electrode material for supercapacitor application. In this present work, Co-doped SnO_2 has been synthesized by a low temperature hydrothermal method and the role of the Co ion in the

* Corresponding author. Fax: +82 62 530 1909.
E-mail address: leeys@chonnam.ac.kr (Y.S. Lee).

0022-3697/$ - see front matter Crown Copyright © 2011 Published by Elsevier Ltd. All rights reserved.
doi:10.1016/j.jpcs.2011.09.026

nanoparticles and its electrochemical properties have been studied.

2. Experimental

2.1. Synthesis of materials

Pure and Co-doped SnO_2 nanoparticles were prepared by a low temperature hydrothermal method. For pure SnO_2 particle preparation, stoichiometric amounts of tin chloride were added to 50 mL of 0.1 M NaOH and stirred thoroughly to achieve a clear solution. Twenty minutes later, 2.0 mM of cetyltrimethyl ammonium bromide (CTAB) powder was added to the above solution, followed by heating to affect complete CTAB dissolution. Then, the mixture was poured into a stainless Teflon-lined 150 mL autoclave and maintained at 150 °C for 24 h. After cooling to room temperature, the resulting precipitate was collected by centrifugation, washed several times with ethanol, and dried at 60 °C for 12 h to yield the SnO_2 nanoparticles. The same method was adapted to prepare Co-doped SnO_2, where $SnCl_4 \cdot 5\,H_2O$ and $CoCl_2 \cdot 6\,H_2O$ were used as respective tin and cobalt ion sources.

2.2. Characterization and electrochemical characterization

Powder X-ray diffraction patterns were recorded between 10 and 80° in an X-ray diffractometer (Rigaku, Rint 1000, Japan), with Cu-Kα as a radiation source. Fourier transform infrared spectroscopy (FT-IR) was performed on an IR Prestige-21 (Shimadzu, Japan) spectrophotometer using a pellet containing a mixture of KBr and the active material in the region of 400–2000 cm^{-1}. The morphology of the carbon was examined by a (Hitachi S-4700, Japan) field emission scanning electron microscope and field emission transmission electron microscope (Tecnai-F20, Philips, Netherland).

Electrodes for the supercapacitors were prepared by the mixing active materials with 20 wt% of a conductive binder and Teflonized acetylene black (TAB) to form a slurry. The slurry was pressed onto a stainless steel mesh (1 cm^2 geometrical area) and dried at 40 °C for 6 h under vacuum. The electrochemical properties of the $Sn_{1-x}Co_xO_2$ composites was investigated by CV with a 3-electrode cell assembly between −0.8 to 0.2 V vs. SCE at various scan rates, namely 10, 25, 50, 75, and 100 mV s^{-1} in 1.0 M H_2SO_4 electrolyte using Zhaner electrochemical measurement units (IM6e, Zhaner, Germany). The prepared electrode was used as the working electrode with a platinum foil serving as the counter electrode and a saturated calomel electrode (SCE) as the reference electrode.

3. Results and discussion

Fig. 1 shows the X-ray powder diffraction patterns of bare and Co-substituted SnO_2 nanoparticles, which infer the phase and purity of the materials. All the diffraction peaks can be perfectly indexed to the rutile structure with a p42/mnm space group (JCPDS-41-1445). It was found that the intensity of the diffraction peaks increased with an increase in the Co content, indicating the difference of X-ray scattering factor between Sn and Co. There were no diffraction peaks observed in any of the patterns due to the Co addition thus elucidating the single phase behavior of the materials as well as the calculated lattice constant values (Table 1) indicating the tetragonal structure of the parent SnO_2 and Co^{2+}-substituted SnO_2. There is little difference observed in the lattice constant with the substitution of Co^{2+} in the SnO_2. This may be due to the closer ionic radii of the Co^{2+} and Sn^{4+} that could occupy regular lattice sites in the SnO_2 [13]. The substitution of Co was little affected in the crystal structure of the SnO_2. The average grain size was calculated using Scherrer formula

$$L = K\lambda/\beta(\cos\theta)$$

Where, K is the constant taken as 0.9, λ the wavelength of the X-ray radiation (Cu-Kα=0.15418 nm) and β the line width at half maximum height at the diffraction angle of θ. The calculated average grain sizes using the (110) diffraction peak was 2 nm for all the samples. It indicates that the there is no significant effect on the grain size due to the doping of Co^{2+} in the SnO_2 structure.

The FT-IR spectrum is an effective tool for characterizing the local cation environment of a lattice containing a closed-packed oxygen array. Fig. 2 shows the FT-IR spectra of the bare and Co-doped SnO_2 nanoparticles. The low wave number region (400–800 cm^{-1}) depicts the lattice vibration of the SnO_2 [14]. The peaks observed at 650, 603, and 561 cm^{-1} were typical for Sn–O stretching vibrations [15]. Similarly, the peak at 3738 cm^{-1} corresponds to the Co–O–Co stretching mode, which is not available in the bare SnO_2. The peak around 1514 cm^{-1} may be due to a small amount of adsorbed water.

Fig. 3 shows the SEM images of bare and Co-doped SnO_2 nanostructures. As shown in the SEM images, the prepared powders were composed mainly of spherical particles with an average diameter of 20 nm, stacked and exhibiting coarse surfaces. In addition, a few large microspheres were also observed. When the addition of Co^{2+} increased in the parent structure, the porous structure and the sizes of the microspheres increased, indicating that the substituted Co^{2+} ion influenced morphology

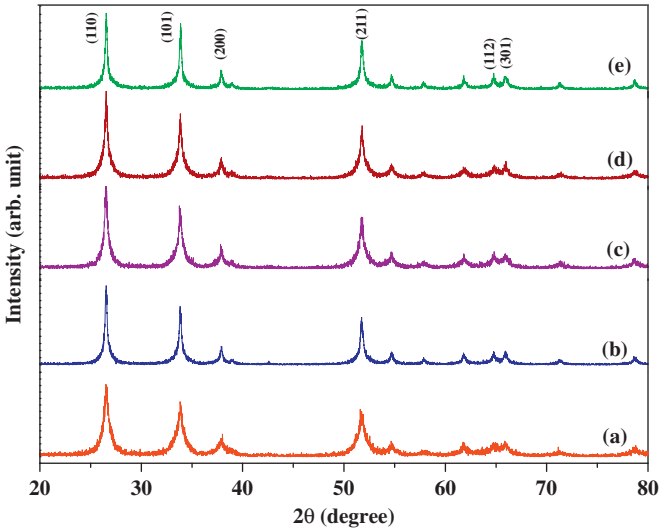

Fig. 1. XRD patterns of $Sn_{1-x}Co_xO_2$: (a) x=0.0; (b) x=0.02; (c) x=0.04; (d) x=0.06; and (e) x=0.08.

Table 1
Structural and electrochemical parameters of Co-doped and un-doped SnO_2.

Sample	Lattice parameters			Specific capacitance at 10 mV s^{-1} (F g^{-1})
	a (Å)	*b* (Å)	*c* (Å)	
SnO_2	4.7494	4.7494	3.1837	742.6
$Sn_{0.98}Co_{0.02}O_2$	4.7483	4.7483	3.1837	733.3
$Sn_{0.96}Co_{0.04}O_2$	4.7411	4.7411	3.1858	840.1
$Sn_{0.94}Co_{0.06}O_2$	4.7433	4.7433	3.1829	720.3
$Sn_{0.92}Co_{0.08}O_2$	4.7482	4.7482	3.1854	814.2

to make the porous structures. Fig. 4 displays the TEM images of the resultant metal oxide nanopowders. The TEM picture revealed that the products were mainly well-dispersed submicron-spheres

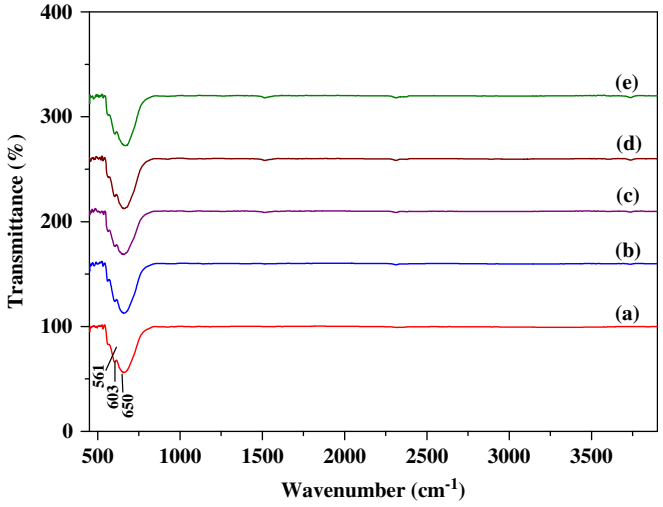

Fig. 2. FT-IR patterns of $Sn_{1-x}Co_xO_2$: (a) $x=0.0$; (b) $x=0.02$; (c) $x=0.04$; (d) $x=0.06$; and (e) $x=0.08$.

indicating a high crystallinity of the materials. The outer surface was constructed of many small nanoclusters that had been rapidly grown from the center of the spheres and resulting in the formation of the hierarchical structure. The size of the composite particles also decreased with an increase in cobalt content. Addition of cobalt acted as the hindering agent, preventing agglomeration of the powders that can confine the effects on particle size. This effect is an important phenomenon for a material to provide excellent electrochemical capacitance behavior during the charge-discharge process.

Cyclic voltammetry was considered an effective route to determine the capacitive behavior of any material. Fig. 5 shows the CV curves of pure and Co-doped SnO_2 particles recorded at a 10 mV s^{-1} scan rate. The CV was carried out between the potentials ranging from −0.8 to −0.1 V in a 1.0 M H_2SO_4 electrolyte. All curves showed rectangular-like shapes within the measured potential window, which is the typical characteristic of capacitive behavior for any material. The SnO_2 is a well-known semiconductor with an optical band gap of 3.6 eV and an electrochemical potential window comparable to the optical band gap. This can be calculated from the CV curves by calculating the potential difference between the cathodic and anodic onset potential values. The capacitive behavior of nanosemiconductor materials in an aqueous electrolyte has been attributed to the

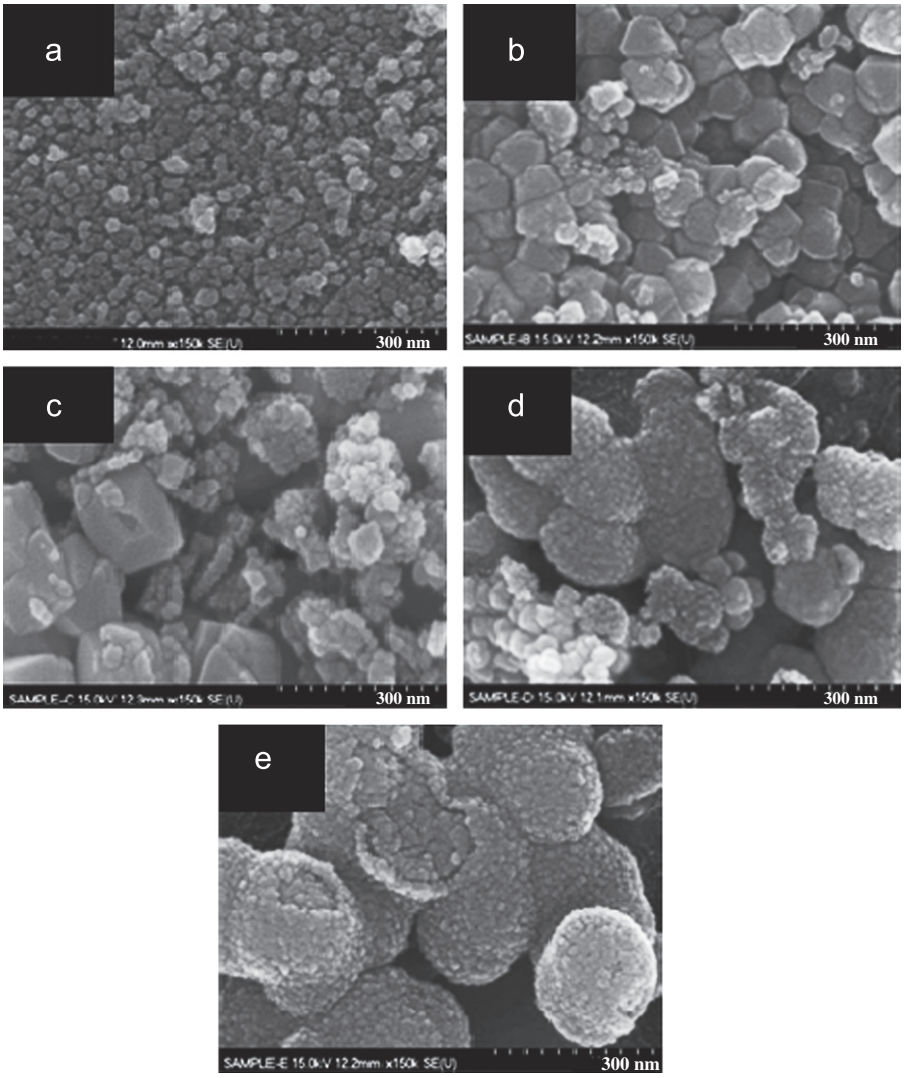

Fig. 3. SEM images of $Sn_{1-x}Co_xO_2$: (a) $x=0.0$; (b) $x=0.02$; (c) $x=0.04$; (d) $x=0.06$; and (e) $x=0.08$.

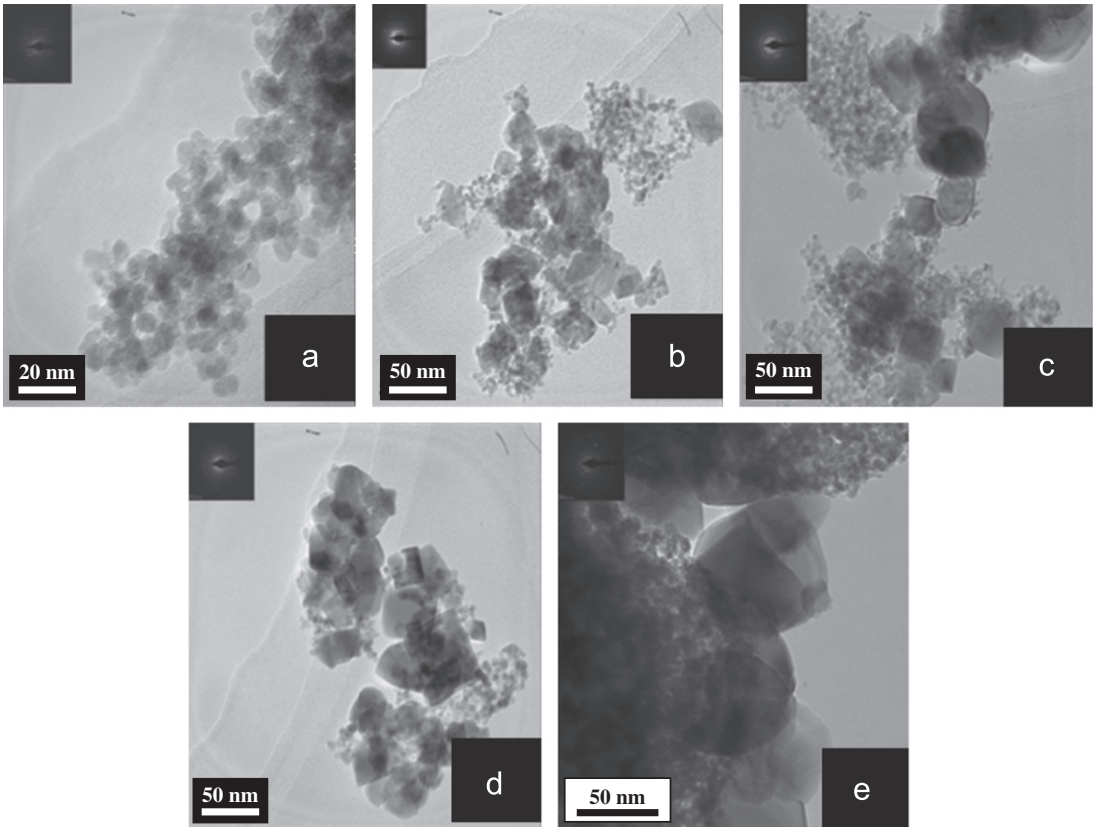

Fig. 4. TEM images of $Sn_{1-x}Co_xO_2$: (a) $x=0.0$; (b) $x=0.02$; (c) $x=0.04$; (d) $x=0.06$; and (e) $x=0.08$.

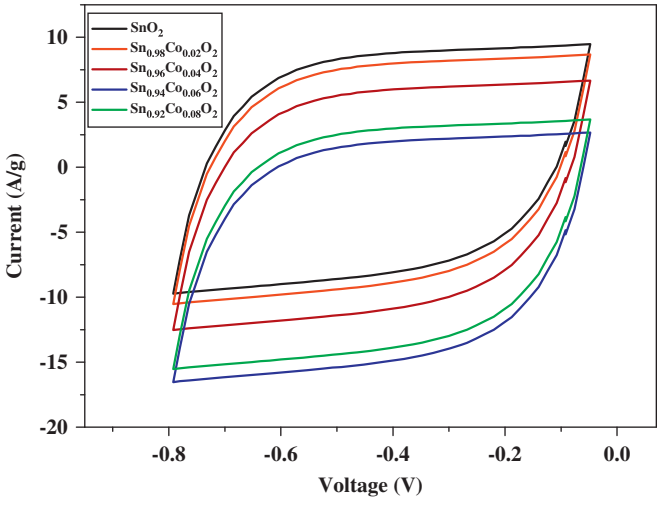

Fig. 5. Cyclic voltammetry curves of pure and cobalt-doped SnO_2.

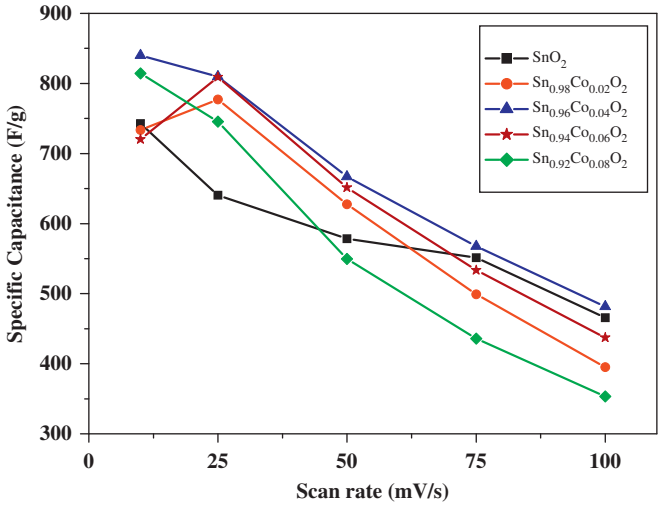

Fig. 6. Dependence of specific capacitance as a function of scan rate.

potential-dependent intrinsic capacitance associated with the electronic state distribution. The specific capacitance ($F\,g^{-1}$) was calculated from the CV curves according to the following equation:

$$C_{sp} = I/S^{*}m$$

where I is the current density (A), s the scan rate ($mV\,s^{-1}$), and m the mass of the electrode active material. The obtained specific capacitance for pure and cobalt-doped SnO_2 materials has been shown in Table 1. A maximum specific capacitance of $840\,F\,g^{-1}$ was obtained for the $Sn_{0.94}Co_{0.06}O_2$ composite metal oxide at a lower scan rate of $10\,mV\,s^{-1}$. Similarly, a specific capacitance of approximately $480\,F\,g^{-1}$ was obtained at a high scan rate of $100\,mV\,s^{-1}$ for the same composite material. The high capacitance value may be due to the high crystallinity of the product and the cobalt doping, as well as the porous morphology [16], confirmed by XRD and TEM. The cobalt doping increased the crystallinity of the products and the mobility of the charge carriers, further increasing capacitance. The obtained specific capacitance values were higher than the reported values of the SnO_2 synthesized by other wet chemical techniques [17–19].

Fig. 6 shows the effects of scan rate on SC of pure and cobalt-doped SnO_2 measured in the potential range of -0.8 to -0.1 V. The capacitance values decreased with an increase in scan rate, which is the typical behavior of an electrochemical system. The main factors influencing the total specific capacitances variation with scan rate are: (1) the decrease in specific capacitances with increasing scan rate was attributed to the reduced diffusion rate of the ions in the pores at higher scan rates. The increase in scan rate directly reduced the ion diffusion, since at high scan rates the ions approach only the outer surface of the electrode material [19]. (2) The surface adsorption process at high scan rates. This is based on the diffusion effects of the proton within the electrode material. Hence, it is held that part of the surface of the electrode materials contribute to a high charging/discharging rate, which decreased the specific capacitance at higher scan rates [20].

4. Conclusion

Nanocrystalline pure and Co-doped SnO_2 with hierarchical structures have been prepared by a simple hydrothermal method. The XRD patterns indicate that the SnO_2 crystallites with a tetragonal rutile structure formed directly during the hydrothermal process without calcination. The SEM and TEM images show that the obtained samples were spherical and well dispersed with a narrow size distribution. The electrochemical properties of the composite metal oxides were evaluated by cyclic voltammetry. The CV curves showed that the synthesized materials possess typical capacitance behavior within a potential range from -0.8 to -0.1 V in a 1.0 M H_2SO_4 solution. A maximum specific capacitance of 840 F g^{-1} was obtained for $Sn_{0.96}Co_{0.04}O_2$.

Acknowledgements

This work was supported by the grant from the Technology Innovation Program of the Ministry of Knowledge Economy of Korea (Project No. K1002176).

References

[1] B.E. Conway, Electrochemical Supercapacitors, Scientific Fundamentals and Technological Applications, Kluwer Academic/Plenum Publishers, New York, 1999.
[2] J.P. Zheng, T.R. Jow, J. Electrochem. Soc. 142 (1995) L6.
[3] H.H. Kim, K.B. Kim, Electrochem. Solid State Lett. 4 (2001) A62.
[4] J.K. Chang, W.T. Tsai, J. Electrochem. Soc. 150 (2003) A1333.
[5] D. Belanger, X. Ren, J. Davey, F. Uribe, S. Gottesfeld, J. Electrochem. Soc. 147 (2000) 2923.
[6] F. Fusalba, P. Gouerec, D. Villers, D. Belanger, J. Electrochem. Soc. 148 (2001) A1.
[7] H.C. Chiu, C.S. Yeh, J. Phys. Chem. C 111 (2007) 7256.
[8] J. Zhu, S.T. Aruna, D. Aurbach, A. Gedanken, Chem. Mater. 12 (2000) 2557.
[9] D.N. Srivastava, S. Chappel, O. Palchik, A. Zaban, A. Gedanken, Langmuir 18 (2002) 4160.
[10] H.Y. Jin, Y.H. Xu, G.S. Pang, W. Dong, J. Mater. Chem. Phys. 85 (2004) 58.
[11] J. Hays, A. Punnoose, R. Baldner, M.H. Engelhard, J. Peloquin, K.M. Reddy, Phys. Rev. B 72 (2005) 075203.1.
[12] N.L. Wu, Mater. Chem. Phys. 75 (2002) 6.
[13] L.M. Fang, X.T. Zu, Z.J. Li, S. Zhu, C.M. Liu, L.M. Wang, F. Gao, J. Mater. Sci. 19 (2008) 868.
[14] Z. Miao, Y. Wu, X. Zhang, Z. Liu, V. Han, K. Ding, G. An, J. Mater. Chem. 17 (2007) 1791.
[15] S. Fujihara, T. Maeda, H. Ohgi, E. Hosono, H. Imai, S.H. Kim, Langmuir 20 (2004) 6476.
[16] D. Deng, J.Y. Lee, Chem. Mater. 2008 (1841) 20.
[17] K. Prasad, N. Miura, Electrochem. Commun. 6 (2004) 849.
[18] C. Hu, C.C. Wang, K.H. Chang, Electrochim. Acta 52 (2007) 2691.
[19] K. Karthikeyan, V. Aravindan, S.B. Lee, I.C. Jang, H.H. Lim, G.J. Park, M. Yoshio, Y.S. Lee, J. Alloy Compd. 504 (2010) 224.
[20] R. Kalaiselvan, I. Perelshtein, N. Perkas, A. Gedanken, J. Phys. Chem. C112 (2008) 1825.